Simulation of the Erosive Effects of Multiple Particle Impacts in Hypersonic Flow

GEORGE C. LORENZ*
The Boeing Company, Seattle, Wash.

An erosion test technique was developed by modifying a 12-in.-diam, hypersonic wind tunnel so that sand and glass beads could be injected into the tunnel flow. Drag computations based upon spherical particle drag indicate particle velocities, dependent upon size of 2550 to 3250 fps. The test specimens made of ablative materials were subjected to either an ablative or a combined ablative-erosive stream. The cloud distribution in the test core was calibrated with a specially designed sampler. Using this calibration, the amount of material impinging upon the model position could be readily determined. The surface temperature of the model was elevated above the normal recovery temperature by a surrounding radiant furnace. Some conclusions of this study were: a slight amount of contamination can increase the total weight loss by a factor of 10; erosion is highly dependent upon surface temperature; a virgin surface is more resistant than one that is charred; the erosion loss increases proportionally with the mass of impinging material; and when the cloud density increases, the loss ratio decreases, approaching an asymptotic value.

Nomenclature

A = particle area, ft²
C_d = particle drag coefficient (dimensionless)
C_N = erosion loss, joules per gram removed
D,F = drag and force, lb
g = gravitational constant, ft/sec²
K = particle velocity component normal to surface, fps²
k = ratio of specific heats (dimensionless)
M = Mach number (dimensionless)
MW = model or specimen weight, g
m = particle mass density, slug/ft³
Re = Reynolds number (dimensionless)
r = particle radius, ft
T = temperature, °F
V = velocity, fps
v = particle residual parallel velocity component, fps
W = dust weight, lb
WR = wear, g
α = impingement angle, deg
γ = particle specific weight, lb/ft³
ϵ = resistance factor for impact wear, ft-lb/g
η = collection ($\eta_c \equiv W_c/W_d$) and/or impingement ratio (dimensionless)
ρ = gas density, slugs/ft³
ϕ = resistance factor for cutting wear, ft-lb/g

Subscripts

A,B = after and before, respectively
AB = ablation
C = collected
Cu = cutting
D = impact
d = dispensed
g = gas
INC = incompressible
i = impinged
o,t = initial and total conditions, respectively
p,s = particle and surface, respectively

Introduction

MISSILE flight through dust clouds induced by nuclear bombs would result in multiple particle impacts on the frontal surfaces of the vehicle. The size of these particles would be dependent upon the time after burst and altitude. Techniques for determining the effects of large particle impacts are well developed.[1] These particles (as small as 0.030 in. diam) can be fired as test specimens from various types of launching devices at velocities up to 50,000 fps. However, the erosive effect of the multiple impacts of micron-sized particles is a different matter. Here the problem becomes one of whether or not excessive structural temperatures occur because of the wear sustained by the heat-resistant covering.

The early work in erosion effects was mostly experimental (circa 1930) and was directed mainly toward sandblasting techniques. Early concern was precipitated by the wear of steam turbine blades caused by condensing water droplets. This problem was compounded when powdered coal was considered as the fuel for railroad gas turbine locomotives. As a result, an experimental program was conducted blowing high-temperature fly-ash on metals representative of turbine blades.[2] Other experiments were being conducted on the gas-solid problem in catalytic cracking plants[3] and sand erosion of hydroelectric water wheel buckets. However, these studies did not develop useful trends toward the basic problem of erosion with respect to heated ablation materials.

In 1958, Finnie analyzed an idealized case of an abrasive grain striking and removing material from a flat surface.[4] He followed this by a more comprehensive article that included an extensive literature search and introduced aerodynamic flow and surface hardness.[5] He developed an abrasion flow apparatus (200–600 fps) and obtained wear data as a function of impingement angle for various metals and glass.[6]

Holtley introduced the concept of attributing the weight loss to impact wear and cutting wear,[7] and Bitter subsequently presented a comprehensive theoretical analysis of both wearing factors.[8] Neilson and Gilchrist expanded Bitter's work with theoretical expressions based upon empirical data.[9] They presented the most meaningful test data and empirical expressions broken down into the impact and cutting wear for various metals and for glass, graphite, and plexiglass. From these data, they developed methods that are fairly applicable to other types of material, including charred cork and carborazole, as described herein. The problem of erosion in rocket motor nozzles is also described by Neilson and Gilchrist.[10]

Rhodes and Bloxom developed an erosion test technique in which a hotshot tunnel accelerates a few micron-sized

Presented as Paper 69-341 at the AIAA 4th Aerodynamic Testing Conference, Cincinnati, Ohio, April 28–30, 1969; received May 13, 1969; revision received October 17, 1969.

* Research Specialist, Aerospace Group. Member AIAA.

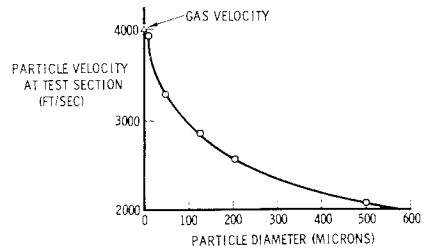

Fig. 1 Computed particle velocities.

particles to velocities above 10,000 fps. These particles strike small test specimens that can be virgin, precharred, or heated by a torch. This technique has recently been expanded, along the principles of the Gatling gun, to permit the firing of a series of particles during a single run.

This paper describes an experimental technique for evaluating erosive effects while simulating the existing aerodynamic heating, flow forces, and simultaneous effects of erosion and ablation. Particles are introduced into the flow of a hypersonic wind tunnel, which drag-accelerates them to velocities up to 3250 fps before they strike specimens of ablative materials. Specimen surface temperature, particle size, and impingement angle, condition of the surface char, and particle mass and density are varied.

Experimental Program

Analytical Preparation

Initial efforts to measure particle velocity showed that the usual and ordinary photographic techniques would not suffice. Since it appeared that an accurate and reliable velocity measurement system would be quite costly, it was decided that the particle velocities would be based on the computed values. Later calculations of the sensitivity of computed velocities to uncertainties in the drag coefficients showed that the variation in computed velocities was small for a realistic range of variation of drag coefficients.

The particles were injected into the wind tunnel approximately 18 in. upstream of the throat. Since they were injected downstream, and the gas velocity in this region is low (50 to 85 fps), it was assumed that the particles at the beginning of the converging section attained this same velocity, V_{p_0}. It was also assumed that they were not affected by gravity. The force acting upon the particles is drag:

$$F = D = [\rho(V_g - V_p)^2 A C_d]/2 \quad (1)$$

and the particle is accelerated to a velocity approaching that of the gas:

$$V_p = \int[(V_g - V_p)^2 A C_d/2m]dt + V_{p_0} \quad (2)$$

$$V_p = \int[3\rho(V_g - V_p)^2 C_d g/8\gamma r]dt + V_{p_0} \quad (3)$$

Here the particle radius r and density γ are given constants, and the gas velocity V_g and density ρ are inputs dependent upon flow conditions within the nozzle. After an extensive literature search, the expression derived by Crowe[11] was selected for the computation of C_d,

$$C_d = (C_{d_{INC}} - 2)e^{-A} + [h(M)/k^{0.5}M]e^{(-Re/2M)} + 2 \quad (4)$$

where

$$A = 3.07k^{0.5}(M/Re)g(Re) \quad (5)$$

$$\log_{10} g(Re) = 1.25[1 + \tanh(0.77 \log_{10} Re - 1.92)] \quad (6)$$

and

$$h(M) = [2.3 + 1.7(T_p/T_g)^{0.5}] - 2.3 \tanh(1.17 \log_{10} M) \quad (7)$$

The values of C_d computed with this expression compare favorably with the curves developed from the experimental results of Selberg and Nicholls.[12] Figure 1 shows the computed velocities for the dust material during the subject test.

Model Collection Efficiency

A cloud sampler (described later) was designed to determine the ratio of the impinging material to the total amount of material dispensed into the tunnel. However, since the shape of this sampler and the models differed, the question arose as to whether the model shock and flow patterns would divert an appreciable number of the particles from their original trajectories (see Fig. 2). Therefore, an analysis was undertaken to determine the magnitude of this correction factor.

Using a sharp cone as the critical configuration and with air as an ideal gas, a conical flowfield was developed on the basis of the Taylor-Maccoll equation. The analysis then computed the change in the particle trajectory (using the aforementioned drag equations) and determined which particle would just touch the shoulder of the core. This "edge" particle then establishes the ratio of volumes, which is the desired correction factor. This procedure revealed that the correction factor was 0.999 for a particle with a diameter of 12.5μ. Since 50μ glass beads were the smallest particles used in this test, it is apparent that a collection efficiency correction factor is unity.

Test Facility

The experiments were conducted in the Boeing 12-in.-diam hypersonic wind tunnel (Fig. 3) in Seattle. This blow-down facility has nozzles for Mach 5.0, 6.05, 6.5, and 7.0 flow. The usable flow core diameters are 8 to 9 in. Total pressure and total temperature are 1200 psig and 1000°F, and run time is 1.5 to 2 min. Specimens can be injected and retracted from the test stream through a slot in the bottom of the diffuser. The test chamber shell has three viewing ports for visual observations and photography.

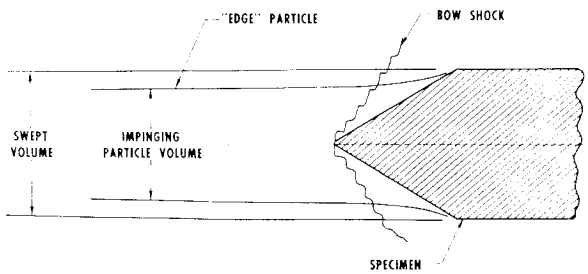

Fig. 2 Model collection efficiency.

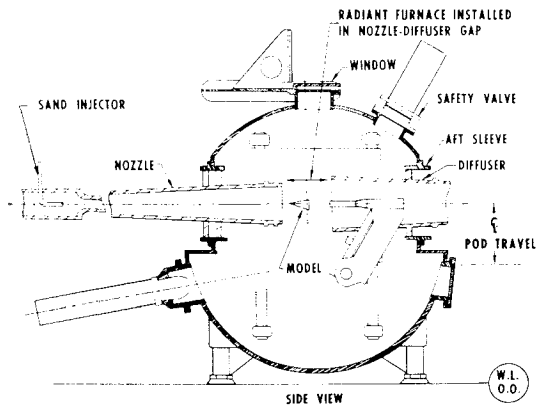

Fig. 3 Modified hypersonic wind tunnel.

The dust injection equipment consists primarily of a pressurized sand storage can with an electrically driven rotary spool at the base. The spool allows a slight advance of the gas flow (high-pressure bottled nitrogen) followed by the dust flow. The latter is regulated by the dome pressure and by the size of the adjustable orifice at the base of the can. The rotating spool also provides for a slight delay in the gas flow at shutdown to allow purging of the delivery tube. The latter runs from the container base through the tunnel wall and bends 90° to a point directly downstream and directly at the throat section. The end of the tube has a four-way opening that disperses the dust particles and is located 18 in. upstream of the throat section. The system pressurization is controlled by a solenoid valve. This valve and the motor driving the rotary spool are controlled by an electric timing device that is accurate to 0.01 sec.

An auxiliary radiant furnace was installed surrounding the entire wind-tunnel test section (Fig. 3), including the slot provided for injection and retraction of the test specimens. It is composed of a water-cooled shell with 76 quartz heating elements lining the inside surface. Its maximum heat flux, 37.5 Btu/ft²-sec, when imposed upon a test specimen in the stream flow, will produce a surface temperature, dependent upon the thermal properties of the material, of ~2500°R. This auxiliary device permits a wide range of surface temperatures for ablation and erosion-ablation testing.

Test Conditions

Tests were conducted under conditions shown in Table 1. Phase I was conducted with the Mach 6.5 nozzle because it was considered to be expendable. Therefore, any damage incurred by the particles passing through the throat would have little consequence. When the damage factor was found to be negligible, testing was switched to the Mach 6.05 nozzle. The total pressure was reduced during Phase II operations, so that the specimen heating rates would be the same in each case. Since the auxiliary furnace was not installed at this time, the specimen surface temperatures would have been 1300° to 1350°R.

The Phase III tests were conducted to resolve a wind-tunnel contamination problem incurred during the AGM ablation testing. These tests required surface temperatures in excess of 1350°R, and as a result led to the design and installation of the radiant furnace. The total pressure was raised to 1000 psig to generate the highest wall shear possible.

The variation in Mach number and total pressure had a slight effect upon the test section gas velocity and a negligible effect upon the test section particle velocities.

The two main factors associated with the simulation of a dust cloud are the mass density and the size of the particles. A range of particle sizes typical of those expected in nuclear dust clouds was selected. A convenient contaminant with a mean diameter of 125μ was found to be an olivine casting sand. For larger particles, a silica casting sand with a mean size of 210μ was selected. Finding an earth-like material of a smaller size proved to be more difficult; therefore 50μ glass beads were substituted.

Table 1 Tunnel test conditions

	Phase I	II	III
Mach number	6.5	6.05	6.05
Gas velocity, fps	4020	3800	3960
Total pressure, psig	1150	850	1000
Total temperature, °R	1460	1460	1460
Re/ft $\times 10^{-6}$	8.0	7.2	8.5
Pressure altitude, kft	80	70	67
Radiant heating, Btu/ft²-sec	None	None	To 38

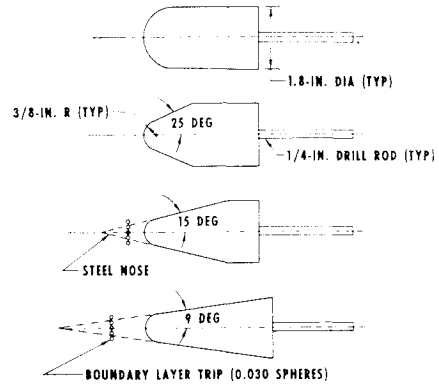

Fig. 4 Erosion models.

Model Design

The four configurations tested are shown in Fig. 4. Each had a 1.8-in.-diam base, a dimension which coincided exactly with the opening in the cloud-sampling device. The sharp-nosed versions had a boundary-layer trip strip consisting of 0.030 steel balls spot-welded with a spacing of one diameter. This trip strip ensured the existence of a turbulent boundary layer over the surface of these cones. All of the cones were molded around a sting mount made of quarter-in. drill rod.

The models were made of three materials; cork, Dow Corning DC-93-072 silicone rubber, and carborazole. The only models instrumented were a group of 9° cones made of silicone rubber. These specimens had four U-shaped foil thermocouples molded at specific depths, 0.010 to 0.050 in. below the surface. These models were used to determine the surface temperatures of the silicone rubber specimens when they were subjected to the combined effects of tunnel flow and external radiant heating.

Test Procedure

Because of particle stratification in the tunnel flow, concurrent specimen testing and cloud sampling were not reliable and feasible. Therefore, many repetitious cloud sampling runs were conducted. These runs included a horizontal and vertical cloud survey to determine the best model location. The average of these runs provided a reliable ratio between the material impinging to the amount dispensed ($\eta_i = W_i/W_d$). After considerable experimentation a dispensing technique was developed where η_i was repeatable within 5%. It was then assumed that this η_i also prevailed during a specimen run; an η_i was determined in this manner for each of the three particle sizes tested.

The cloud sampler design that proved to be the most effective is an L-shaped tube with the short leg open and the long leg closed. The open end, equipped with a hardened steel nose-ring, was positioned in the tunnel flow. Particles flowing down the nozzle and into the test section passed through the sampler bow shock, entered the tube, and were collected at the closed end. At the conclusion of the run, the material collected was removed from the sampler and weighed. Therefore, $\eta_C = W_C/W_d$ was established for each particle size.

The specimens were tested by ablation, ablation-erosion, and surface-temperature runs. In the ablation runs, they were simply exposed to the tunnel flow, or combined tunnel flow-radiant heating conditions, for a specific length of time. Ablation-erosion runs were conducted using three initial surface conditions: 1) hot-char, 2) cold-char, and 3) virgin or uncharred. A hot-char run is made by exposing the specimen to the test environment for a specific time (usually 10 sec) prior to exposure to the dust cloud. This mode

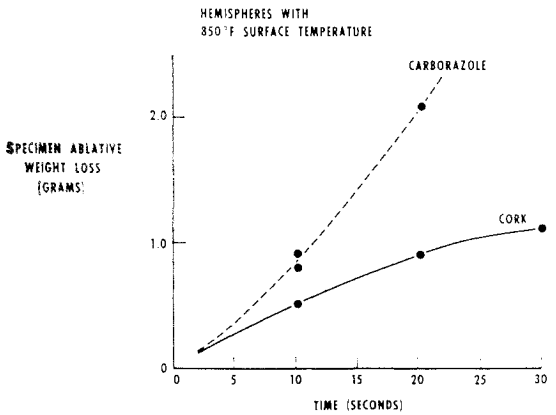

Fig. 5 Ablative weight loss.

represents missile entry into the dust cloud at the higher altitudes and hotter portion of the trajectory. In a cold-char run, a previously charred but not eroded specimen is exposed to the dust cloud at the instant the model arrives at the tunnel centerline. This mode results in a concurrent reheating and erosion of the char; it is used to permit evaluation of the relative resistances of hot and cold chars, not to simulate flight conditions. Finally, a run using a new uncharred specimen represents missile entry into a dust cloud at lower altitudes while the missile is still relatively cool; charring and erosion occur concurrently.

In the surface-temperature runs, silicone rubber models were exposed to the combined effects of tunnel flow and radiant heating. Each model was run with an increase in the radiant heat flux until the maximum level of 37.5 Btu/ft²-sec was achieved. Thermocouples were installed at four surface depths in the specimens.

Data Reduction

The weight of dust or sand dispensed into the tunnel was determined by placing a 300-g sample in the sand storage can prior to a run and weighing the residue after the run ($W_d = 300 - W_A$). The amount of sand presumed to have impinged upon a specimen, W_i, was the product of W_d and η_C, as described previously. The loss of material due to stream and radiant heating effects was determined by simple "before and after" weight measurements: $MW_{AB} = MW_B - MW_A$. The ablation-only losses, as a function of time, for cork and carborazole are shown in Fig. 5.

Ablation-Erosion

The specimen material lost during an ablation (prechar) interval followed by erosion is also a measurement of before and after weights. To obtain the weight loss due to erosion alone, one can either subtract just the prechar ablative losses, or subtract the ablative loss for the entire exposure period. For example, if a model were subjected to 10 sec of prechar and 10 sec of erosion, the pretest weight could be

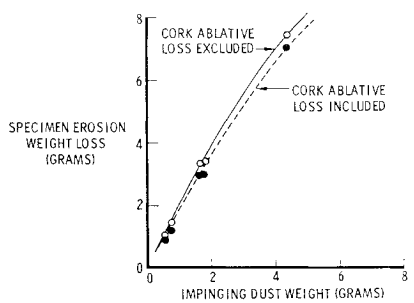

Fig. 6 Comparison of analysis methods.

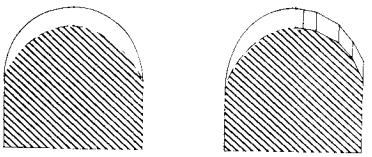

Fig. 7 Modified hemisphere for Neilson-Gilchrist analysis.

reduced by either 10 or 20 sec of ablative weight loss, per Fig. 5. Neither approach is absolutely correct, because during the erosion phase the losses are due to the combined effects of ablation and erosion. However, since the two effects cannot be separated and extended prechar ablative loss data are not available for all specimen configurations, method 1 above has been used in the analysis of these data. The effects of including and excluding the weight loss can be seen in Fig. 6, where the data for the hemisphere models for each method are shown.

A profile-measuring device, referred to as a comparator and comprising a spark gap generator, a collimating mirror, and a polaroid film holder, was devised to record specimen shape changes. The before and after profile shadows of the specimens were projected upon the film by the short-duration spark. Thus, a black profile of the remaining configuration was superimposed upon a gray profile of the original shape.

Wear Analysis

Some of the hemispherical cylinder erosion data were analyzed using the method of Neilson and Gilchrist.[9] In this work, the authors have developed a simple approach to a theoretical analysis of the general erosion problem. The derived equations are correlated by experimental results and can be used to predict the erosion characteristics of various materials. The total erosive wear sustained by a specimen can be subdivided into cutting wear and impact wear,

$$WR_t = WR_{Cu} + WR_D \tag{8}$$

and

$$WR_t = m(V_p^2 \cos^2\alpha - v_p^2)/2\phi + m(V_p \sin\alpha - K)^2/2\epsilon \tag{9}$$

where WR_t is the erosion produced by m pounds of particles impinging at an angle α and with a velocity of V. The term K is the velocity component normal to the surface below which no erosion takes place, and v_p is the residual parallel component of particle velocity at low α's. Because of the large magnitude of V in the tests, K and v_p are assumed to be negligible in comparison and are dropped from Eq. (9).

Now, at $\alpha = 90°$, the first part of the expression, cutting wear, is zero and the impact resistance constant ϵ is determined by

$$\epsilon = (mV_p^2)/2WR_t \tag{10}$$

After ϵ has been obtained, the impact wear at all angles can be determined, and by subtracting it from WR_t, WR_{Cu} and the cutting resistance constant ϕ can be obtained.

Some of the hemisphere cylinder data were reduced by this method using comparator photographs as shown in Fig. 7. The hemispherical surface was divided into segments, the recession measured, and the shape transformed into a series of trapezoids. The volume of each revolved trapezoid can be determined, and with the resulting volume ratio, the weight loss of each part can be found. Using a similar approach, the swept area can be ratioed and the amount of dust impinging on each segment can be determined. From this, the eroded weight-impacted weight ratio for each segment is resolved.

Now, all of the quantities in the wear equation are known except ϵ and ϕ. The impact factor ϵ was obtained from the center segment where $\alpha \simeq 90°$. The α for each of the other

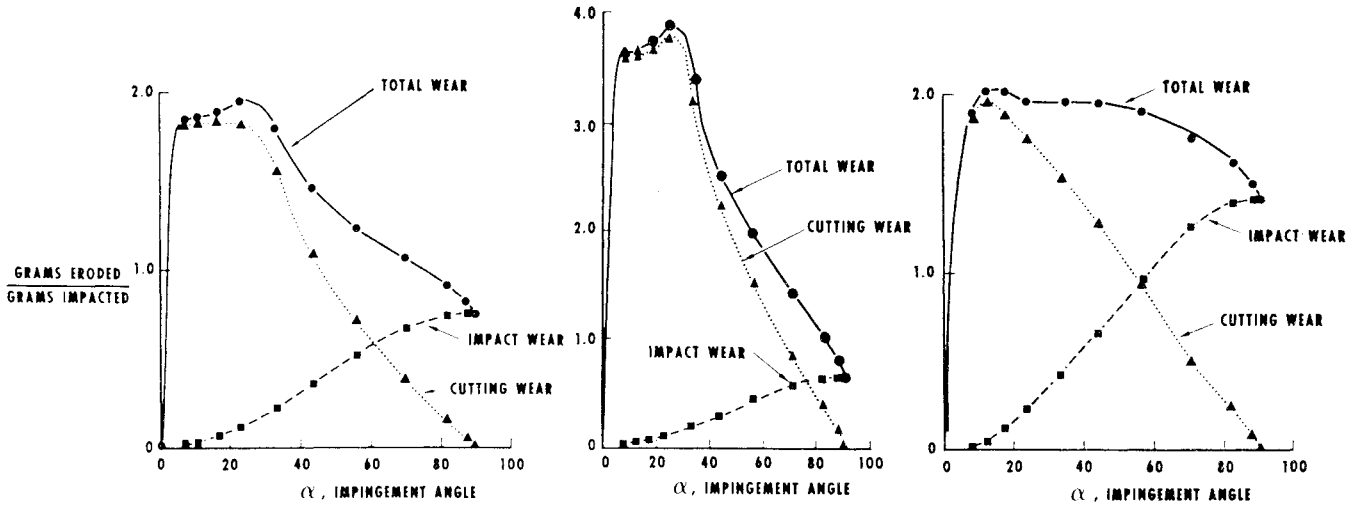

a) 50μ glass beads, V = 3250 fps b) 125μ olivine sand, V = 2850 fps c) 210μ silica sand, V = 2550 fps

Fig. 8 The effect of impingement angle on erosion ratios for 850°F charred cork.

segments was the average across the face of the trapezoid. With this approach, the total wear can be resolved into its two components and the angle of maximum wear can be obtained. Therefore, an approximation of the material's relative resistance to impact and cutting wear can be derived. A computer program was developed and some of the specimens were analyzed by this method. The results are shown in Figs. 8 and 9.

Surface Temperature Extrapolation

The temperatures recorded by the four foil thermocouples embedded in the instrumented silicone rubber models were plotted, as a function of depth, temperature, and time, for each of the radiant heat flux rates. One of the resulting plots of specimen surface temperature vs time is shown in Fig. 10.

The symbol C_N is often used in expressing a degree of erosion loss in joule/g of material removed. The data shown herein can be expressed in terms of C_N by the use of the equation

$$C_N = 4.63 \times 10^{-5} V_p^2/LR \qquad (11)$$

where the loss ratio LR is the specimen weight loss divided by the weight of the impinging dust.

Test Results

The dramatic increase in the erosion rate of Dow Corning DC-93-072 silicone rubber as the surface temperature T_s is elevated from 850° to 1800°F is shown in Fig. 11a. The erosive effects are rather insignificant for $T_s \lesssim 1000$°F; the material acts essentially as the tough virgin material. However, at $T_s > 1000$°F, the rubber surface begins to take on the appearance of a dried "mud flat" and becomes rather soft and brittle, susceptible to particle impact. The effect of slight contamination is notable in the cross-plotted data of Fig. 11b, where an impaction of 0.5 g results in an increase of specimen weight loss of several factors, e.g., 5 at 1500°F. These same data are presented in Fig. 12, where the total specimen weight loss is normalized by the uncontaminated ablation loss, revealing that the effect of increasing the particle impingement rate diminishes as T_s is elevated beyond 1200°F. This can be attributed to the increasing significance of the pure ablation loss as the surface temperature is elevated beyond 1200°F.

The effects of elevated T_s on the erosion of cork by particles are shown in Fig. 11c. Because cork forms a surface char at a lower T_s than silicone rubber, it shows a relatively high loss ratio at 850°F. At 1250°F, the only other data point, the cork loss ratio increases by a factor of 2 to 3. However, the curve indicates that as the particulate mass density increases, the char is removed faster than it is formed and the loss ratio approaches an asymptote. The elevated temperature data for cork are limited to this one curve, and no tests were conducted with carborazole at elevated temperatures.

The effect of particle size on the weight loss incurred by the cork and carborazole hemispheres can be noted in Fig. 13a. The data for 125μ and 210μ particles fall on the same loss ratio line, but the erosion weight loss is notably smaller for the 50μ glass data. The latter was unexpected because one could anticipate that the greater surface area-to-mass

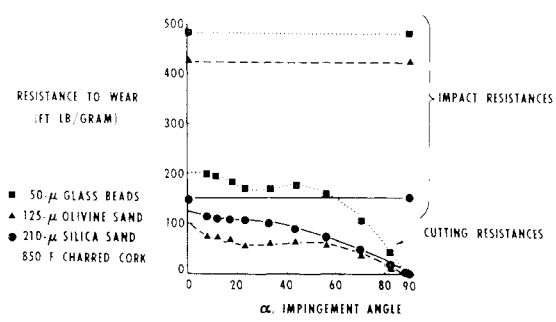

Fig. 9. The effect of impingement angle on material resistance.

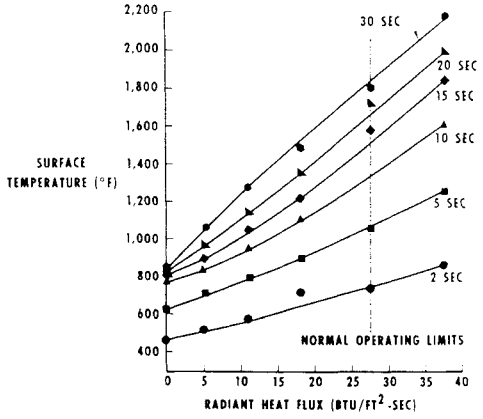

Fig. 10 Silicone rubber model surface temperature

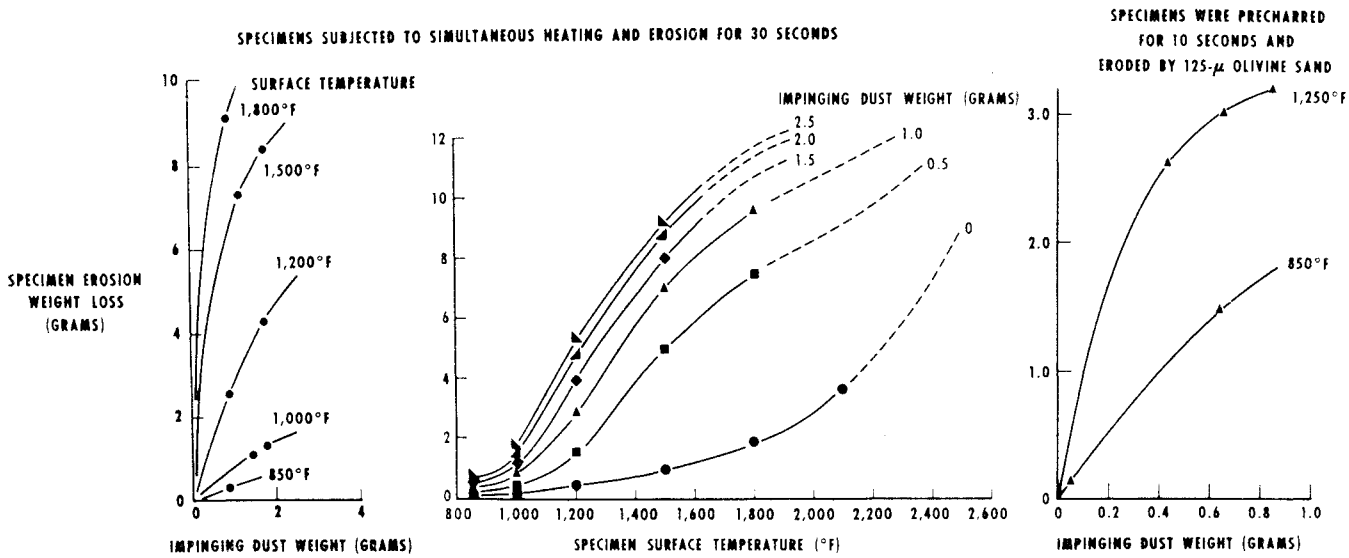

a) 9° silicone rubber cone b) 9° silicone rubber cone c) 15° cork cone

Fig. 11 Weight loss of sharp cones eroded by 125μ olivine sand.

ratio would result in an increasing volume removal per unit mass of abrasive. However, considering the analytical method of Finnie,[5] it would appear that at similar energy levels, angular particles should produce more erosion than spherelike particles. This is confirmed by test data from Ref. 13, where sandblasting with "sharp" sand produced four times the wear of round sand. Viewed through a microscope, the 125μ olivine sand and 210μ silica sand are angular, and the glass beads are spherical and smooth. Therefore, the effect noted in these data may be due more to the particle shape rather than to size.

Figure 13 also shows that at the 850°F surface temperature condition, the carborazole is slightly more resistant to the sand particles, and considerably more resistant to the glass beads, than is cork. This figure also shows that the virgin silicone rubber has superior abrasion resistance at these low surface temperatures.

The testing of impingement angle was limited to angles between 9° and 25°, because the missile surfaces protected by these ablation-insulation materials are essentially within these limits. Figure 13b is a result of tests conducted with cone specimens with half-angles of 9°, 15°, and 25°. The data verify the previously noted effects that carborazole is slightly more resistant than cork and also that the smaller glass beads produce less wear, but impingement angle has very little effect, especially where the more extensive data exist for the larger particle sizes. The cork and carborazole

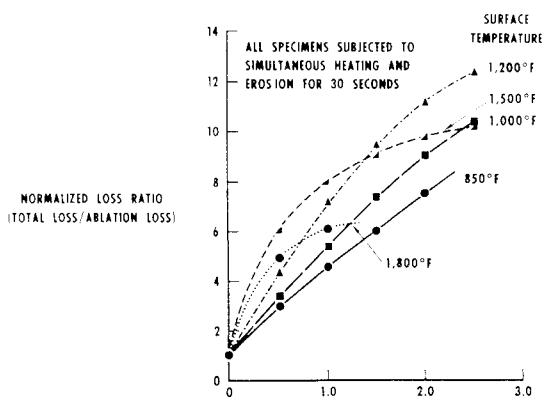

Fig. 12 Normalized weight loss of a 9° silicone rubber cone.

data show loss ratio curves where all three cone angles lie within the limits of experimental error. The limited data with the glass beads more vaguely indicate that the 15° angle is more susceptible in carborazole, while the 9°-angle is more critical in cork, but these effects are small.

Some of the hemisphere data were reduced by the procedures outlined in Ref. 8. The analysis (described heretofore), leads to an empirical solution for the angle producing the maximum total wear rate. These solutions indicate that the maximum wear curves for cork and carborazole are very flat between $\alpha = 10°$ and $\alpha = 30°$; thus, the analytic results also fail to reveal a critical α among those tested.

With respect to surface conditions, Fig. 14 shows that for cork, the virgin surface is most resistant, followed by the cold-char and hot-char, respectively. For the carborazole specimens, the loss ratio was essentially the same regardless of the surface condition, probably because the sticky or tacky nature of this char more closely resembles that of the virgin material.

A good example of the effect of cloud dust density or mass density on the loss ratio is seen in the 1250°F curve of Fig. 11. These data were generated in the same test mode: a 10-sec period of char followed by 10 sec of dust. However, the total amount of dust dispensed was different for each run, producing the curve in the data. As discussed earlier, this would indicate that as the cloud density or impingement rate is increased the char is removed as fast as it forms. Therefore, the loss ratio curve should approach the asymptotic value that would exist for the virgin unheated material. However, since the mass density values used in this experiment were consistent with those anticipated in a nuclear cloud, it is doubtful that this would ever happen in actual flight.

The effect of changing the impinging mass while maintaining a constant cloud density (i.e., holding a constant dispenser output setting and operating it for varying lengths of time) is seen in Fig. 13. The weight eroded is nearly a linear function of the impinging mass.

Conclusions

1) A dust cloud with a contamination density close to predicted values can increase the weight loss in an ablative-insulative material, such as cork or silicone rubber, by a factor of 5 to 10.

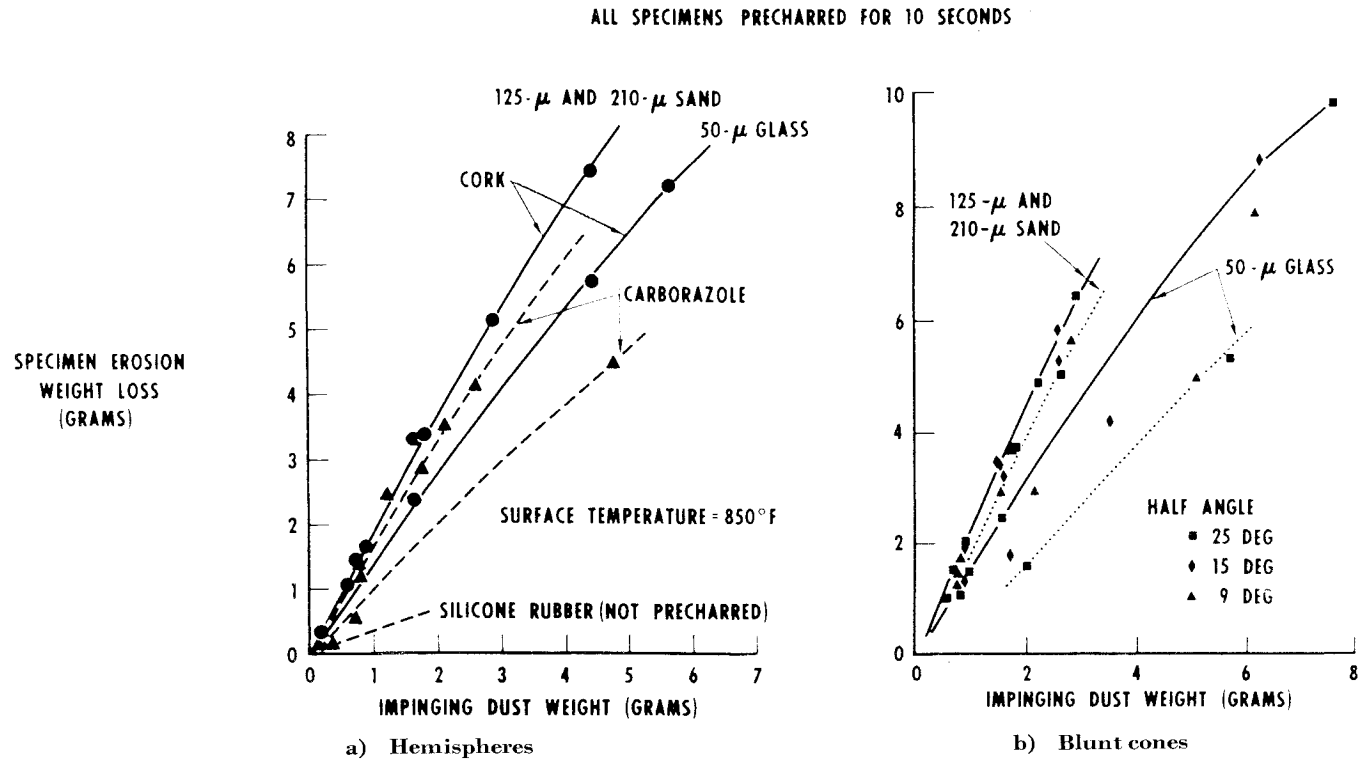

Fig. 13 The effect of particle size on the erosion weight loss of cork and carborazole.

2) The erosion loss ratio is highly dependent upon the surface temperature and material characteristics. The silicone rubber used in these tests appeared to have a resistance threshold at 1000°F, beyond which the loss ratio is greatly accelerated. Cork appears to have similar characteristics at a lower temperature; however, data are insufficient to predict the exact temperature threshold.

3) The virgin uncharred material is the most resistant to erosion. If a char already exists on the surface of a cork specimen when the erosion process begins, an initially cold char is more resistant than a hot char.

4) With the cloud contamination density held constant (within predicted limits), the weight of material eroded increases in direct proportion with the mass of the impinging material.

5) When the cloud particle density is increased, the erosion loss ratio decreases approaching an asymptotic value that could be established with uncharred virgin material.

6) Analysis of the hemisphere data by the method of Neilson and Gilchrist indicates that charring cork exhibits the general characteristics of a material like plexiglass. With this method the relationship between the impact wear and cutting wear was determined.

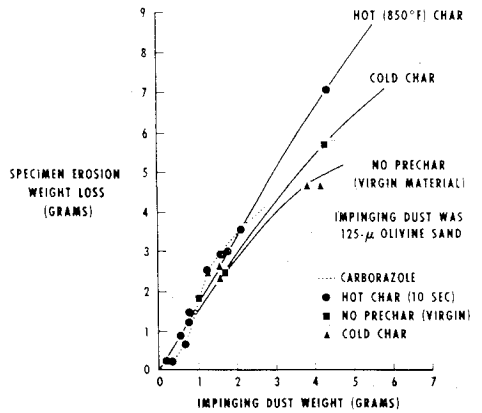

Fig. 14 The effect of char on the erosion weight loss of cork and carborazole hemispheres.

7) The tests conducted with cones with different half-angles produced no clear evidence of an effect of impingement angle in the 9°–25° range. The analysis of the hemispheres by the procedure of Neilson and Gilchrist[8] substantiates this conclusion by revealing very flat loss ratio curves between impingement angles of 10° to 30°.

References

[1] Belton, W. L., Gideon, D. N., and Stein, R. A., *Hypervelocity Impact Data Index, Part I—Bibliography*, Rept. BAT-197A-21-2 (Rev. 2), Jan. 1967, Battelle Memorial Institute, Columbus, Ohio.

[2] Fisher, M. A., and Davies, E. F., "Studies of Fly-Ash Erosion," *Transactions of the ASME*, Vol. 71, No. 6, June 1949, pp. 481–487.

[3] Stoker, R. L., "Erosion Due to Dust Particles in a Gas Stream," *Industrial and Engineering Chemistry*, Vol. 41, No. 6, June 1949, pp. 1196–1199.

[4] Finnie, I., "The Mechanism of Erosion of Ductile Metals," *Proceedings of the 3rd U.S. National Congress of Applied Mechanics*, Pergamon Press, London, 1958.

[5] Finnie, I., "Erosion of Surfaces by Solid Particles," *Wear*, Vol. 3, Feb. 1960, pp. 87–103.

[6] Finnie, I., "An Experimental Study of Erosion," *Proceedings of the Society of Experimental Stress Analysis*, Vol. 17, No. 2, Feb. 1968, pp. 65–70.

[7] Holtey, H., "Über den Abnützungsvorgang in Blasversatzzrohren und die Frage der Bekampfung des Verschleisses," *Geologie und Mijnbouw*, Vol. 1, 1939, p. 209.

[8] Bitter, J. G. A., "A Study of Erosion Phenomena," Pts. 1 and 2, *Wear*, Vol. 6, Jan. 1963, pp. 5 and 169.

[9] Neilson, J. H. and Gilchrist, A., "Erosion by a Stream of Solid Particles," *Wear*, Vol. 11, No. 2, Feb. 1968, pp. 111–122.

[10] Neilson, J. H. and Gilchrist, A., "An Experimental Investigation into Aspects of Erosion in Rocket Motor Tail Nozzles," *Wear*, Vol. 11, No. 2, Feb. 1968, pp. 123–143.

[11] Crowe, C. T., "Drag Coefficient of Particles in a Rocket Nozzle," *AIAA Journal*, Vol. 5, No. 5, May 1967, pp. 1021–1022.

[12] Selberg, B. P. and Nicholls, J. A., "Drag Coefficients of Small Spherical Particles," *AIAA Journal*, Vol. 6, No. 3, March 1968, pp. 401–408.

[13] Rosenberg, S. J., "Resistance of Steels to Abration by Sand," *Transactions of the American Society of Steel Treating*, Vol. 18, 1930, p. 1093.